Experimental Investigation of Bio-Reactive Transport at the Continuum Scale for Underground Hydrogen Storage

Gerald Stiedl[1,*], *Patrick* Jasek[1], and *Holger* Ott[1]

[1]Montanuniversity Leoben, Department Geoenergy, 8700 Leoben, Austria

Abstract. This study examines dispersive and bio-reactive transport processes in porous rock relevant to underground hydrogen storage and in-situ methanation. Experiments were conducted in a custom-designed core flooding facility equipped with medical X-ray computed tomography (CT) and gas chromatography (GC) to characterize reactive transport in sandstone core samples. Reservoir conditions were replicated by cultivating anaerobic methanogenic microorganisms in a reactor and subsequently inoculating the cores. A series of dispersion experiments was performed to investigate mixing between resident and injected gas phases. The presence of a water phase increased system complexity by introducing gas solubility effects and reducing gas saturation while modifying heterogeneity (introducing macro tortuous pathways), thereby influencing dispersion and the local composition of the injected gas constituents. For the dry H_2-N_2 system, an effective diffusion coefficient of $1.75 \cdot 10^{-7}$ m²/s was determined. Bio-reactive conversion consumed H_2 and CO_2 while producing CH_4, resulting in methane formation rates of 0.178-0.284 mmol L^{-1} h^{-1}. Microbial activity further reduced core permeability by approximately 50%, demonstrating the strong coupling between transport processes and microbial methanation.

1 Introduction

The transition toward a decarbonized energy system necessitates the large-scale storage of renewable energy to bridge the gap between fluctuating supply and demand. Underground Hydrogen Storage (UHS) in depleted natural gas reservoirs and deep saline aquifers has emerged as a primary solution due to the high storage capacities of these geological formations. However, the efficiency of UHS is significantly influenced by complex reactive transport processes. As hydrogen is injected into the subsurface, it interacts with the initially equilibrated system, comprising residual reservoir gases, formation brine, and indigenous microbial communities, leading to phenomena such as molecular diffusion, dispersion, and biochemical reactions.

A critical challenge in evaluating potential storage sites is quantifying the dispersive mixing of H_2. Advective dispersion and molecular diffusion generate concentration gradients that affect the purity of the recovered gas and, thus, the economic feasibility of UHS operations. Understanding these transport mechanisms is essential for predicting the spatial distribution of fluids, which in turn dictates the loss of recoverable hydrogen

In addition to the losses caused by irreversible dissipative processes, initial field-scale pilot projects have demonstrated that microbial metabolism can contribute to the reduction of reproducible hydrogen [1], [2]. Especially in porous storage formations, such as depleted gas reservoirs, the reduction of stored hydrogen can be elucidated by biochemical reactions induced by methanogenic archaea[3], [4]. The metabolism of these microorganisms, which are residing in the pore space of the reservoir rock, converts H_2 together with CO_2 as a carbon source into methane and water according to the so-called Sabatier reaction:

$$4H_2 + CO_2 \rightarrow CH_4 + 2H_2O \qquad (1)$$

This, in terms of hydrogen storage efficiency detrimental impact, yields a new approach to efficiently store excess renewable energy in the form of "renewable" methane. The process of microbial conversion of H_2 and CO_2 into methane can be considered as a form of CCU (carbon capture and utilisation), where atmospheric CO_2 (direct air capture) or more highly enriched CO_2 from industrial point sources can be utilised.

While the potential in terms of available formations for geo-methanation is high, the process is coupled with physical changes in the reservoir. The anaerobic bio-methanogenesis is controlled by the concentration of available substrates, salinity, pressure and the presence of competing microorganisms in the formation water [5]. Increasing reaction rates are inevitably associated with the formation of biomass. The extensive growth of biofilms can lead to bio-clogging, which can alter the hydraulic properties of the formation, specifically reducing porosity and permeability [6], [7], [8].

The success of in situ gas conversion is fundamentally governed by the composition and metabolic productivity of the methanogenic archaea present in the reservoir. Characterizing the factors that regulate microbial activity is therefore vital for predicting the performance of these subsurface bio-reactors.

* Corresponding author: gerald.stiedl@unileoben.ac.at

A sufficient nutrient supply in the form of the injected gas is essential for the bioreaction driven by the microbial population, which is residing in the aqueous phase within the pore space. With regard to conventional hydrogen storage, the CO_2 concentration initially in place as well as in the injected gas stream has proven to be a critical factor for methane conversion and the purity of the reproduced hydrogen. The produced-to-injected hydrogen ratio and the amount of recovered hydrogen is strongly controlled by the amount of CO_2 in the injected stream, whereas the amount of generated methane is more influenced by the initial CO_2 conditions [2]. Ultimately, the local concentration of these essential gaseous nutrients is influenced by diffusive and dispersive transport mechanisms during gas displacement, which are the primary focus of this investigation. To accurately model these large-scale reservoir processes, precise laboratory-scale quantification of transport coefficients is required.

The displacement of the initially resident gas by the invading gas stream is affected by dissipative processes, i.e., irreversible dispersive flow, which causes mixing and spreading of the gas constituents. This process, referred to as hydrodynamic dispersion, results in temporal and spatial variations in gas composition. Hydrodynamic dispersion is commonly described by the advection-dispersion equation (ADE), which is derived from the principle of mass conservation. With an additional source or sink term (Q), which encompasses all processes that locally generate, consume or convert a quantity, independent of transport, it is also known as the advection-dispersion-reaction equation (ADR) and can be formulated as follows [9], [10], [11]:

$$\frac{\partial}{\partial t}\mathrm{C} = \mathrm{D}\nabla^2 C - \mathrm{u}\nabla\mathrm{C} + Q \qquad (2)$$

According to Eq. 2, mass transport can be decomposed into a conservative advective component, represented by the second term on the right-hand side, and a dissipative component associated with random transport processes, represented by the first term containing the second spatial derivative. The dissipative term comprises contributions from molecular diffusion and hydrodynamic dispersion. While molecular diffusion is generally independent of the flow rate, hydrodynamic dispersion results from spatial variations in fluid velocities within the pore network and therefore depends on the local velocity field. The scaling factor by which the mechanical dispersion increases with flow velocity is called dispersivity (α). In the following, the combined effect of molecular diffusion and hydrodynamic dispersion is referred to as dispersion, and the term dispersion is used to describe both processes collectively. When considering depleted gas fields as hydrogen storage sites, both a gas phase and an aqueous phase must be taken into account, comprising a connate water phase and, potentially, an underlying aquifer. Since the solubility of individual gas components in the brine phase depends on their partial pressures and, consequently, on their concentrations in the gas phase, hydrodynamic dispersion also influences the amount of dissolved gas components [12], [13], [14]. Dissolved nutrients in the liquid phase must then be transported to the locations where microorganisms reside. The efficiency of substrate transport in the liquid phase depends on the average distance between the gas-liquid interface and zones of biomass accumulation, as well as on the dominant transport mechanism, i.e., is the transport advective or diffusion-dominated.

To systematically analyse this complex problem, dry gas-gas displacement tests were carried out in the first step. On the one hand, these are intended to demonstrate the capabilities of the experimental setup and, on the other hand, to serve as a basis for subsequent experiments with increased complexity.

The introduction of a stationary water phase is expected to influence dispersive transport by reducing the pore space available for gas flow, altering flow-path tortuosity, and promoting gas dissolution. These effects are investigated in this study, with particular emphasis on their impact on the transport characteristics of different gas constituents.

As a next level of complexity, the presence of an active microbial population in the liquid phase was established. Through their metabolism, gases can not only be dissolved into the liquid phase until a certain solubility limit is reached, according to the biochemical reactions, various components can also be removed from the gas phase beyond that limit. In addition to the consumption of the injected gas components and the associated change in dispersivity, a change in the distribution of the water phase is also expected as water-binding biomass accumulates. Conversely, the dispersion influenced distribution of the nutrient gases can have a significant effect on the conversion rate and growth of biomass.

2 Experimental setup and data acquisition

2.1 Concept and design of the core flooding facility

The custom-designed core flooding setup is schematically displayed in Fig. 1. Within the core holder, cylindrical rock samples with a length of up to 100 cm and a diameter of 1.5 or 3 inches can be mounted Fig. 2. The core holder is horizontally positioned in a medical CT scanner. The confinement fluid surrounding the sealing sleeve is pressurized by an automated cycling pump. The confinement fluid is heated, and the circulation allows the core sample to be continuously maintained at the desired experimental temperature with an accuracy of $\pm$ 1 °C. To force the working fluids through the core sample and to prevent bypassing, the confinement pressure was set 50 bar above the working pressure at any time.

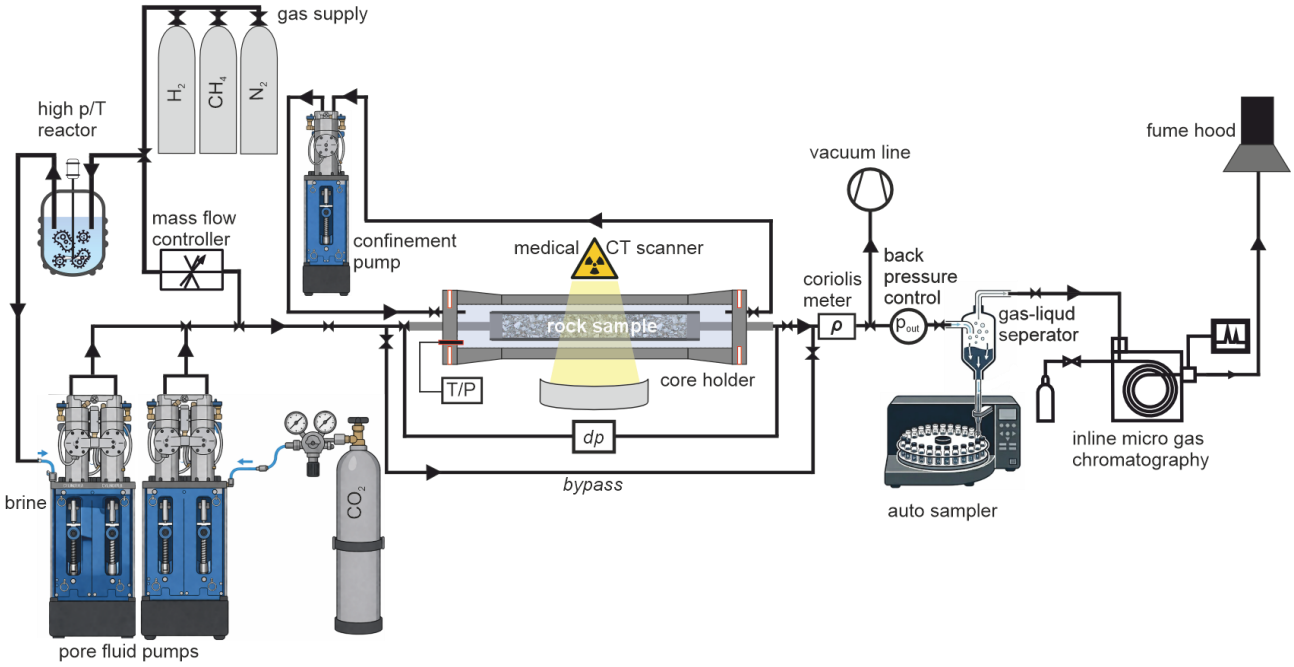

Fig. 1: Schematic of the experimental core flooding setup with the core holder unit, medical CT-scanner, and confinement loop; inlet side (left): metering pumps for injection of liquids and microbial suspensions (grown in high p/T reactor), thermal mass flow controller for gas injection; outlet side (right): inline Coriolis meter, backpressure system, and micro GC.

Liquids and supercritical fluids are injected via high-pressure metering pumps (Vindum Engineering) with constant flow rate or at constant pressure. Gaseous components are injected with defined flow rates via calibrated thermal mass flow controllers (Bronkhorst EL-FLOW series). At the outlet side, a back-pressure system is mounted to adjust the pore pressure in the core. The accuracy of the diaphragm-controlled pressure regulator is within 1 - 2 % under the experimental conditions and flow rates. The detailed performance curve can be found in [15]. Absolute pressure measurements at the inlet and outlet tubes, as well as a differential pressure measurement via a pressure transducer, enable the monitoring of the hydraulic properties of the system during the experiments. Additionally, a Coriolis meter (Bronkhorst mini CORI-FLOW series) is installed to log the density of the effluent stream, which gives information about the current chemical or phase composition of the produced fluid.

After the pressure relief at the outlet, the gas and liquid phases are separated. Produced liquids can be frequently sampled for further analysis. The gas stream is directly fed into an inline micro gas chromatography system (Agilent 990 Micro GC system) for time-resolved chemical analysis of the effluent gas. To obtain a more accurate measurement of hydrogen concentration in the gas phase, a Clark-type hydrogen sensor (Unisense, Aarhus, Denmark) was installed. The sensor measures the hydrogen concentration in the effluent gas phase via hydrogen partial pressure with a detection limit of 0.037 vol%.

A more detailed description of the experimental setup and an exact specification of the core holder unit can be found in [16].

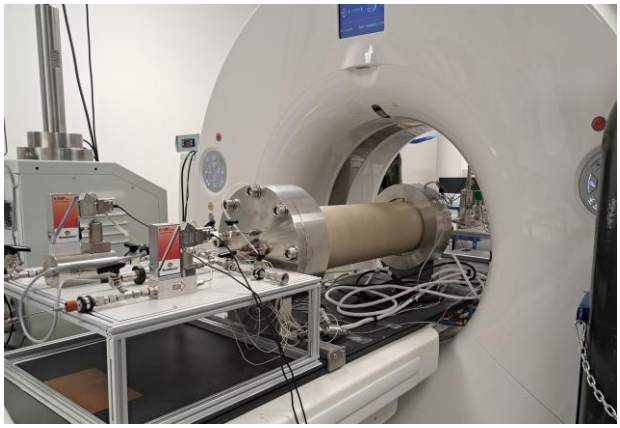

Fig. 2: Image of the core flooding setup placed on the CT scanner table

2.2 Data acquisition and evaluation

To obtain reliable, robust outcomes from individual experiments, temporal and spatial information must be compiled and superimposed.

The core holder unit is placed and aligned on the movable table of a medical computed tomography scanner. With a standard medical resolution of 300 µm in the x/y plane and 600 µm along the z-axis, the entire core can be displayed. The CT scanner was operated in single-energy mode with an acceleration voltage of 120 kV.

Via differential scanning method porosity distribution and the spatially and time-resolved fluid phase saturations can be measured. The image reconstruction of the CT-scanner converts the attenuation coefficients μ of each pixel into numerical values, so-called CT numbers. These numbers are normalized to the attenuation coefficient of water. Their unit is called Houndsfield units (HU). To evaluate the saturation of fluid A displacing fluid B at a given time (Eq. 3), in addition to the actual scan (CT^{i}_{Core}), reference scans of the core fully saturated ($S_\alpha = 1$) with the displacing fluid $\alpha = A$ ($CT^{A,sat}_{Core}$), and with the displaced fluid $\alpha = B$ ($CT^{B,sat}_{Core}$) are required. The time dependent saturation maps can then be calculated as follows [17], [18]:

$$S^{i}_{A}(\vec{x},t) = \frac{CT^{Bsat}_{Core}(\vec{x}) - CT^{i}_{Core}(\vec{x},t)}{CT^{Bsat}_{Core}(\vec{x}) - CT^{Asat}_{Core}(\vec{x})} \qquad (3)$$

In the case of miscible displacement, e.g., between two gases, concentration profiles can be measured instead of phase saturations if the density difference is sufficiently large. With an appropriate scanning interval, concentration profiles over time and the length of the core sample can be recorded.

To calculate the porosity of the rock, the CT values of the pure fluids used to saturate the core must be measured (HU_i). Using the fully saturated core sample scans (CT^{isat}_{Core}), the porosity can be calculated as follows:

$$\phi(\vec{x}) = \frac{CT^{Bsat}_{Core}(\vec{x}) - CT^{Asat}_{Core}(\vec{x})}{HU_B(\vec{x}) - HU_A(\vec{x})} \qquad (4)$$

Based on the geometric dimensions of the core sample and its porosity, the total pore volume can be calculated. The gas pore volume is determined by considering the average water and gas phase saturations across the entire core. To ensure comparability between the individual dispersion experiments, the injected gas volumes were normalized to the gas pore volume (PV_{Gas}). At a constant injection rate, lower gas saturations result in higher flow velocities and vice versa. The specified injection rates, initially given in ml/min at standard conditions (0 °C, 1 atm), were converted to experimental conditions and divided by the volume available for the gas phase within the core.

Fig. 3 the average porosity profile along the x-axis, alongside the distribution of the water phase within a 1.5-inch sandstone core prior to a dispersion experiment. Before the test, the core sample was inoculated with methanogenic microorganisms. Due to the negligible density contrast, the biophase cannot be distinguished from the brine phase via CT imaging. Prior to the commencement of the experiment, the depicted saturation configuration was established by flushing the sample with an inert gas. Reference scans conducted before and after the experiment indicate that the water phase distribution remained nearly constant and can thus be considered stationary.

The three-dimensional distribution of porosity (grey) and gas saturation (red) is visualized in Fig. 4. With the installed inline micro-GC unit, an accuracy of retention time standard deviation (RSD) of less than 0.25% can be achieved for qualitative determination and quantitative analysis, with a response RSD of less than 1% [19]. The in-situ density measurement accuracy using the Coriolis flow meter has a relative deviation of ± 0.5% [20]. Regarding medical CT scanner measurements, Vinegar

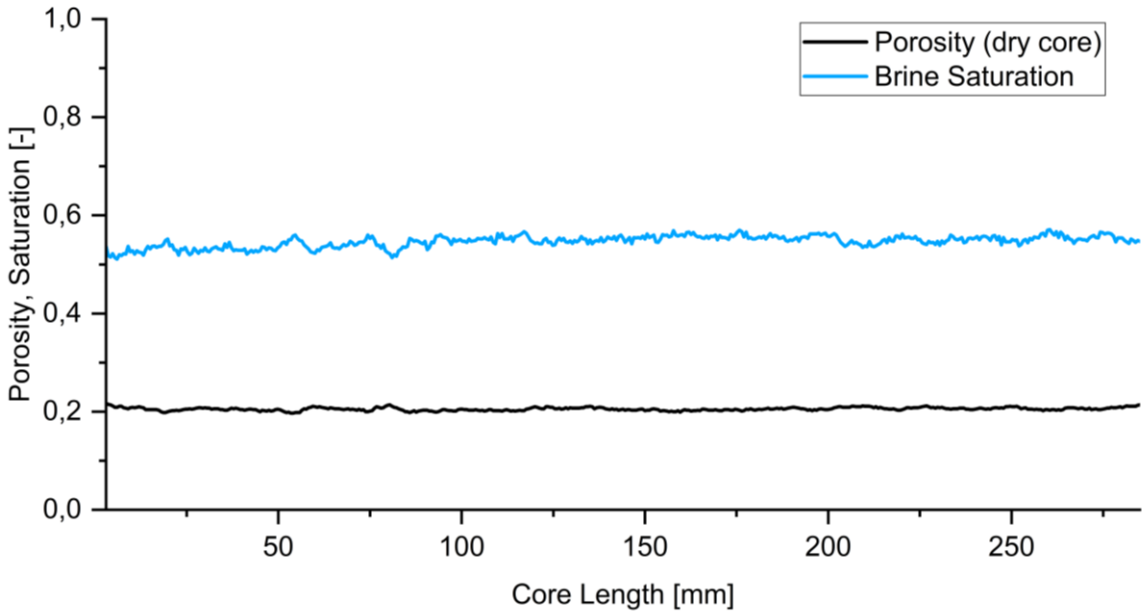

Fig. 3: One-dimensional profiles of the brine saturation (blue line), gas saturation (red line), and the porosity of the dry core (black line) acquired vis difference scanning

and Wellington [21] characterised the sensitivity to saturation changes in multiphase flow experiments using single- and dual-energy modes. With a measurement accuracy of ± 1 HU, changes in saturation could be identified with an accuracy of ± 1% in single-energy scanning operations. As the scanner used in this study has a comparable measurement accuracy, and as the concentrations and saturations are calculated according to the same principle, it can be assumed that the accuracy is in the same range. For medical applications, the manufacturer specifies a practical tissue distinguishability of 3 HU [22]. This corresponds to an absolute saturation accuracy of 3% in this case.

experimental period. Pressure and temperature were kept constant during this process. For initial testing purposes, pure components (N_2, CO_2, H_2) were used. In the next stage, gas mixtures were also injected. From the perspective of efficient nutrient supply for the microbial consortium, a mixture of H_2 (10 vol%) and CO_2 (2.5 vol%) in Ar (87.5 vol%) was used as the displacing fluid. Argon is used in this mixture as a non-oxidising inert gas.

These experiments are designed to observe displacement reactions and dispersion behaviour of the gaseous components in porous media. Furthermore, the influence of a stationary aqueous phase compared to dry core

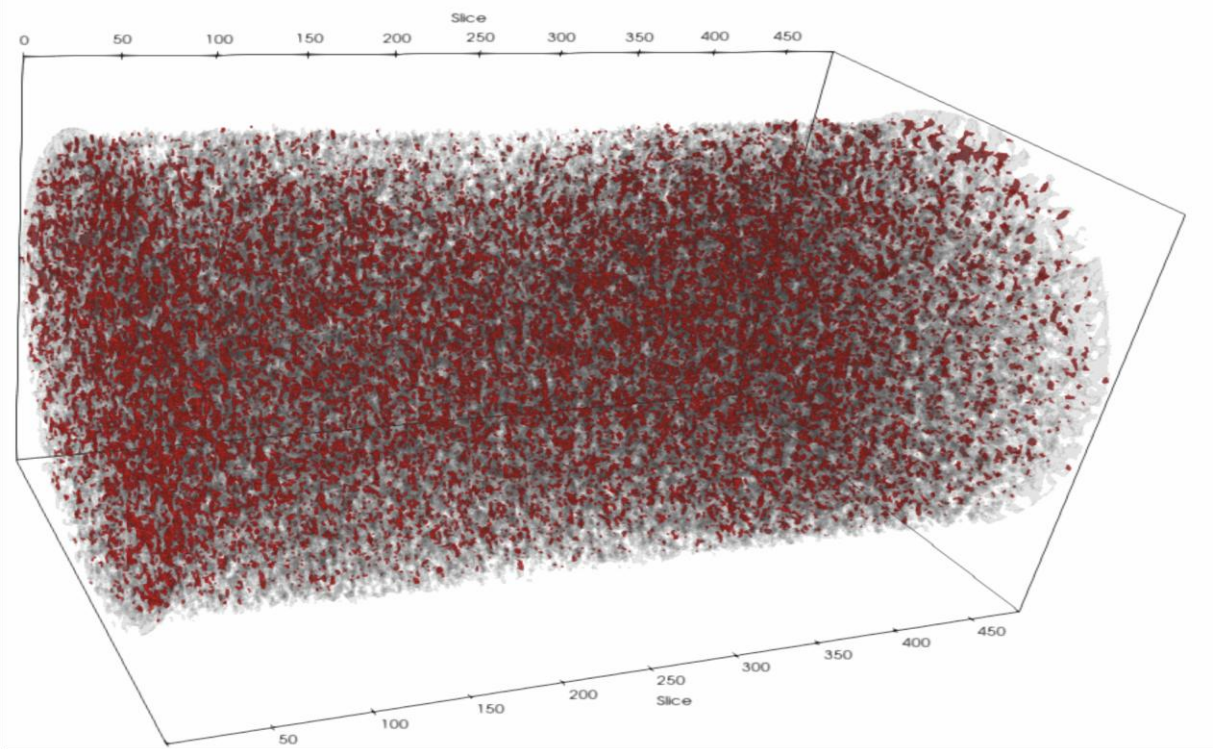

Fig. 4:Three-dimensional illustration of the porosity distribution (grey) and the gas saturation (red) prior a dispersion experiment including microbial population

2.3 Experimental procedure

The key task of the experimental work is the performance of core flooding experiments on rock samples under reservoir conditions. These tests are intended to identify physical and chemical mechanisms and evaluate them to make solid statements about their influence on underground hydrogen storage facilities and potential subsurface in situ reactors. Accordingly, certain design criteria are required for the core flooding setup, in order not only to meet safety-related requirements, but also to be sensitive enough to quantify these effects.

Regardless of the test condition of the core sample (dry, with a stationary brine phase or with microbial culture), a homogeneous and pure gas phase was established at the start of the experiment, which was displaced at a constant rate by another gaseous component during the material, as well as the presence of extensively distributed biomass with an active methanogenic metabolism, should be evaluated stepwise.

The experiments were performed using Berea sandstone cores with a diameter of 1.5 and 3 inch and a length of 30 cm. Berea sandstone is a well-sorted sedimentary rock that is widely used as a standard reference material in laboratory studies of porous media [23], [24]. The permeabilities, measured with brine as the fluid agent was in the range of 120 to 250 mD. Porosity measurements via CT scanning showed an average of 0.18-0.25. Test temperature for all experiments were set to 50°C. Dispersion experiments were conducted in dry rock samples as a base case and in a water-saturated core to investigate the influence of the aqueous phase. For the latter experiments, a synthetic brine was prepared. The chemical composition is derived from the microbially active Lehenfeld gas field in Upper Austria [1]. The

complete list of ingredients and their concentrations is reported in [25]. For the present experiments conducted without microorganisms, the organic components are omitted, but to create comparable conditions with respect to the pH values and ion concentrations and thus also the gas solubilities, all inorganic components are exactly adopted. For the gas-dispersion experiments, high-purity H_2 and N_2 (grade 5.0) supplied in standard gas cylinders (Linde Gas) were used. In addition, supercritical CO_2 ($scCO_2$) was injected from a liquid CO_2 cylinder (Linde Gas). The gas used as a nutrient supply for the microbial population was a premixed gas mixture containing 10.000% H_2, 2.500% CO_2, rest Ar (Prüfgasklasse 1, Linde Gas). The following experiments were performed:

Table 1: Overview of conducted experiments

Sample diameter	Saturation-state	Pore pressure	Resident gas	Injected gas	flow rate	Brine saturation	interstitial velocity
inch		bar			mL(N)/min)		m/s
1.5	Dry	100	N_2	H_2	3.3	-	3.08E-06
1.5	Dry	100	N_2	H_2	10	-	9.33E-06
1.5	Dry	100	N_2	H_2	100	-	9.33E-05
3.0	Dry	100	N_2	H_2	10	-	2.33E-06
3.0	Dry	100	N_2	H_2	350	-	8.16E-05
3.0	Dry	100	N_2	H_2	500	-	1.17E-04
3.0	Wet	100	N_2	H_2	10	0.74	8.97E-06
3.0	Wet	100	N_2	H_2	100	0.74	8.97E-05
1.5	Dry	100	$scCO_2$	H_2	3.3	-	3.08E-06
1.5	Dry	100	$scCO_2$	H_2	10	-	9.33E-06
1.5	Dry	100	$scCO_2$	H_2	100	-	9.33E-05
3.0	Dry	100	$scCO_2$	H_2	100	-	2.33E-05
3.0	Dry	80	N_2	10% H_2, 2.5 % CO_2, 87.5% Ar	2.99	-	2.8E-06
3.0	Dry	80	N_2	10% H_2, 2.5 % CO_2, 87.5% Ar	2.99	-	2.8E-06
3.0	Dry	80	N_2	10% H_2, 2.5 % CO_2, 87.5% Ar	2.99	-	2.8E-06
3.0	Wet	80	N_2	10% H_2, 2.5 % CO_2, 87.5% Ar	2.99	0.61	7.2E-06
3.0	Wet	80	N_2	10% H_2, 2.5 % CO_2, 87.5% Ar	2.99	0.535	6.0E-06
3.0	Wet	80	N_2	10% H_2, 2.5 % CO_2, 87.5% Ar	2.99	0.53	6.0E-06
3.0	Wet with microbs	80	N_2	10% H_2, 2.5 % CO_2, 87.5% Ar	2.99	0.555	6.3E-06
3.0	Wet with microbs	80	N_2	10% H_2, 2.5 % CO_2, 87.5% Ar	2.99	0.554	6.3E-06
3.0	Wet with microbs	80	N_2	10% H_2, 2.5 % CO_2, 87.5% Ar	2.99	0.583	6.7E-06

2.1.1 Dry base case

To decompose the bioreactive transport system, a series of experiments with increasing complexity are conducted. With a focus on diffusive and dispersive effects alone, core flooding experiments in dry rock samples were carried out. For this base case scenario, experiments were carried out on Berea sandstone cores, which were dried at 65 °C for over one month before mounted in the core holder unit.

2.1.2 Stationary brine phase

With the introduction of a stationary aqueous phase into the pore space of the core sample, less pore volume is available for the dispersive flow of the gas phase with its components. In addition, mass transfer occurs between the gas and aqueous phases. The extent to which this additional complexity affects the overall transport behavior of the system is investigated through these experiments and by comparison with the corresponding dry reference case.

A particularly developed synthetic formation water was used for the introduction of the aqueous phase in order to (a) simulate the prevailing conditions in real fields as closely as possible and (b) ensure the best possible conditions for the methanogenic consortium to spread and grow in the core sample. The exact composition and the resulting pH value of the formation brine can significantly affect the activity and metabolism of the microbial community. In response to the altering environmental conditions, their primary energy generation through hydrogenotrophic methanogenesis can be replaced by other biochemical conversions.

The synthetic formation water was chosen in view of our intention to carry out experiments with microbial populations. The chemical composition was derived from the microbial active Lehenfeld gas field in Upper Austria [1]. The complete list of ingredients and their concentrations is reported in [25]. For the present experiments without microorganisms, the organic components were omitted, but in order to create comparable conditions with regard to pH value and ion concentrations and thus also gas solubilities, all inorganic components were exactly adopted.

Before the actual gas dispersion experiments are started, synthetic brine is injected under initial vacuum conditions until the core is fully brine saturated. Subsequently, the liquid phase is displaced by (sc)CO_2 with a moderate injection rate (in the order of 1 PV/h). The remaining brine is considered as an immobile phase since the gases subsequently injected for the dispersion experiments have a much lower viscosity than the (sc)CO_2 ($\mu_{scCO2}/\mu_{H2} > 3$), and the gas-brine displacement efficiency is therefore negligible.

2.1.3 Active methanogenic culture

To conduct experiments with active microbial specimens within the rock sample, the installed core must be anaerobically inoculated. The used methanogenic consortia were initially taken from a pilot field site and cultivated in the laboratory [25]. A high-temperature reactor was used to cultivate the microbial culture, to achieve precisely defined and constant conditions. Through analysis of the gas phase and monitoring of the pressure, microbial activity and metabolism could be effectively tracked, allowing for a defined starting condition before the microbial community were used to inoculate the core samples.

To minimize the carry-over of by-products and buffering agents from the bioreactor, a defined volume (2 ml) of the microbial suspension was extracted and transferred into three septum flasks. These flasks were pre-sterilized and prepared with 20 ml of synthetic brine (SB) under a 1.5 bar nutrient gas atmosphere (10 vol% H_2, 2.5 vol% CO_2 and 87.5 vol% Ar). The flasks were stored in an incubator, with the gas atmosphere replaced on a weekly basis.

For the inoculation of the core sample, the microbial solutions were combined with fresh SB medium and transferred into a 500 ml stainless steel cylinder using a high-precision syringe pump (Chemyx Inc., Stafford, Texas, USA). An overpressure was applied to the cylinder using an inert gas (Ar) to inject the microbial suspension into the core. This sequence was performed twice, followed by a shut-in period.

After a one-week shut-in, the core was flushed over several days with a total of 500 ml of SB medium at moderate flow rates (0.01–0.1 ml/min). This procedure was conducted to ensure optimal microbial distribution and inoculation throughout the entire core volume. Over a two-week period, the pressure was incrementally increased to experimental conditions (80 bar) using low nutrient gas supply rates.

3 Results and interpretation

3.1 Dispersion

In the first phase of the experimental work, pure hydrogen gas was consistently employed as the displacing gas. Through gas-gas displacement experiments using N_2 and scCO_2 as displacing agents at different injection rates and flow regimes, dispersion curves were recorded at different Peclet numbers over a range of more than one order of magnitude. The experimentally obtained dispersion curves were quantified by fitting an analytical solution of the 1D advection-diffusion equation. From these fits, dispersion coefficients were determined, and by correlating the dispersion coefficients with the interstitial velocity, the effective gas–gas diffusion coefficient was obtained by linear extrapolation to zero velocity. This value was compared with a generalized empirical equation [26] for binary gas diffusion coefficients,

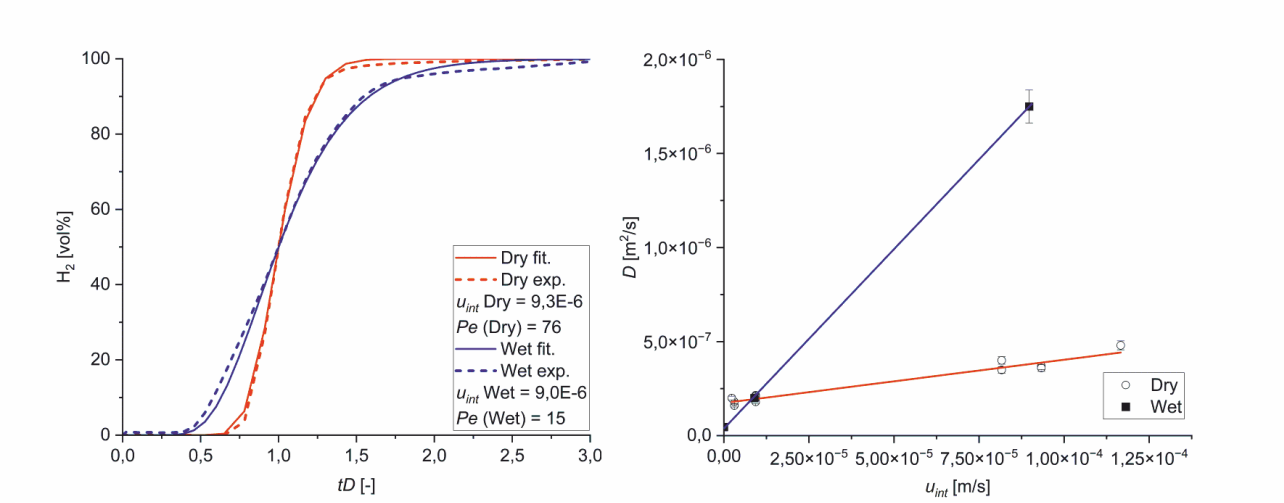

Fig. 5: Left panel: Hydrogen concentration profiles of a dry and a water-saturated dispersion experiment in which nitrogen is displaced with similar interstitial velocities. Right panel: H_2 dispersion coefficient vs. the interstitial velocity for dry and brine saturated (S_b = 0.74) conditions

demonstrating good agreement. Furthermore, the longitudinal dispersivity was derived from the slope of a linear fit.

The results of this initial study, conducted prior to the introduction of microbial culture into the core sample, are detailed in [16]. Based on the linear relationship between the dispersion coefficient and interstitial velocity [11], [27], an effective diffusion coefficient of $1.75 \cdot 10^{-7}$ m²/s was determined for H_2 gas displacing N_2. Under the experimental conditions of 100 bar and 50 °C, [26] yields a bulk diffusion coefficient of $9.3 \cdot 10^{-7}$ m²/s. When taking the pore structure into account [28], an effective diffusion coefficient of $1.55 \cdot 10^{-7}$ m²/s is obtained, which is in excellent agreement with the experimentally determined value.

In addition to the determination of effective diffusion constants, these experiments investigated dispersion behavior as a function of the injection rate and, consequently, the interstitial velocity. A comparison between dry tests and experiments involving an immobile brine phase revealed a flow-rate-dependent impact on the dispersion characteristics.

At low flow rates, compared to the dry case, the reduced effective diffusion coefficient is decisive for the overall lower dispersion behavior of the system. At higher flow rates, the increase in dispersivity dominates and leads to more pronounced spreading of the dispersion curve in the brine-saturated case compared to the dry system at comparable interstitial velocities (Fig. 5 right). The increase in dispersivity may be caused by the reduction in the available pore space (decreasing gas saturation) and the additional contribution of tortuosity due to the presence of the additional phase. The scaling with the reduced gas saturation is sufficient to explain the effective diffusion coefficient, with no noticeable adjustment of tortuosity in the partially saturated case.

Fig. 5 (left panel) shows the hydrogen concentration profiles for a dry dispersion test and a water-saturated experiment in which nitrogen is displaced with approximately the same interstitial velocity. In the wet scenario, the spreading of the concentration profile is significantly more pronounced than in the dry test, which is reflected by a smaller Peclet number and a higher dispersion coefficient.

In the experiments involving microbial cultures within the core samples, a behavior similar to that observed in the presence of an immobile aqueous phase was identified. Within the complete experimental sequence, three dry, three brine-saturated, and three microbially active displacement experiments were conducted. Due to differences in core sample diameter and injected gas composition, a direct comparison with the results reported in [18] cannot be made; however, a comparable overall trend was observed.

Within the selected low-flow-velocity regime, the experiments involving an aqueous phase (sterile brine-saturated and microbially active conditions) exhibited less dispersive behavior compared to the dry core experiments. Similar to the dispersion experiments conducted with pure gases, molecular diffusion represented the dominant dissipative transport mechanism under the investigated flow conditions ($u_{int} = (2.8 - 6.7) * 10^{-6}$ m/s). Consequently, the reduced pore space available for gas transport due to water saturation was identified as the primary factor governing the lower dispersive behavior in the partially brine saturated systems.

Only minor differences were observed between the sterile brine-saturated and the microbially inoculated dispersion experiments. However, to draw robust conclusions regarding the influence of microbial activity on dispersion behavior, further detailed analyses are required, including a comprehensive evaluation of measurement uncertainties and the variability between individual experiments.

3.2 Solubility

The effect of hydrogen solubility was quantified and found to be below 1% of the injected amount, remaining below the detection limit and having no measurable impact on gas composition. Detailed information on the calculation and evaluation of hydrogen solubility can be found in [16]. This behavior undergoes significant modification in the presence of CO_2 within the injected gas stream. A comparative analysis of experiments conducted on dry, brine-saturated (SB), and microbial culture-inoculated cores reveals a distinct shift in the CO_2 breakthrough curves for the latter two cases when compared to the dry dispersion experiment. In all three cases, nitrogen was displaced by the nutrient gas mixture (10 vol% H_2, 2.5 vol% CO_2 and 87.5 vol% Ar).

To determine the solubility of CO_2 within the brine volume present in the core, the Henry's Law constant was calculated at 50 °C [29], [30]. With a given a CO_2 partial pressure of 2 bar (experimental Pressure = 80 bar with a mole fraction of 0.025 CO_2) and brine saturations ranging from 0.5 to 0.6, the maximum theoretical amount of dissolved CO_2 is between 1.26 and 1.52 mmol. All experiments involving an immobile brine phase (with or without active microbial cultures) were conducted within this saturation range.

By normalising the injection rate to the free gas pore volume (PV_{Gas}) of the core sample, the injected gas quantity can be expressed as a fraction of the pore volume that can be occupied by the gas phase. Consequently, the maximum soluble amount of CO_2 is introduced into the core after an injection of 0.56 PV of the gas mixture.

Fig. 6 illustrates a shift of approximately 0.5 PV in the CO_2 breakthrough curves for the brine-containing experiments (blue and green curves) relative to the dry core sample (orange curve). The aforementioned solubility values were calculated for pure water. For water with elevated salinity (seawater [29], [30]), the soluble CO_2 quantity corresponds to a volume of 0.43 PV of the injected gas mixture. In any case, the experimentally measured breakthrough curves exhibit a shift that correlates closely with the solubility of CO_2 in the respective volume of the immobile aqueous phase.

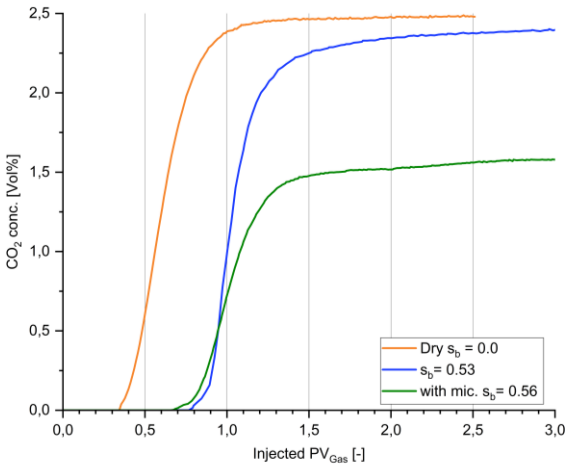

Fig. 6: Comparison of CO2 breakthrough curves for dry (orange), brine-saturated (blue), and microbially active (green) dispersion experiments. The injection rate was maintained at 2.99 mL(n)/min. The injected gas volume was normalized to the free gas pore volume (PV) in accordance with the respective phase saturations.

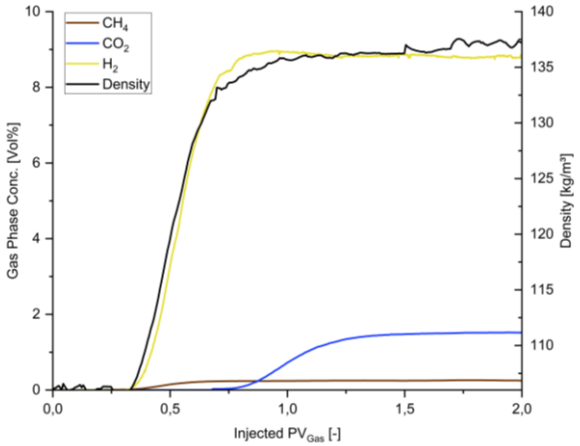

Fig. 7: Gas concentrations at the outlet of a microbially active dispersion experiment with an average gas saturation of 0.44. The secondary y-axis displays the measured gas density. The injection rate was maintained at 2.99 mL(n)/min of the nutrient gas mixture nutrient gas mixture (10 vol% H_2, 2.5 vol% CO_2 and 87.5 vol% Ar) displacing nitrogen. The injected gas volume was normalized to the free gas pore volume (PV) in accordance with the respective phase saturations.

This shift in CO_2 breakthrough at the outlet, relative to H_2, is also evident in the evaluation of individual dispersion tests involving an aqueous phase ($S_b = 0.56$) and microbial cultures (Fig. 7). Although both gases are injected simultaneously at a constant rate at the inlet, the comparatively high solubility of CO_2 results in a retarded breakthrough compared to the barely soluble H_2 [16].

3.3 Microbial Consumption and Metabolic Conversion

Prior to the dispersion experiments involving microbial activity, the microbial culture had to be established within the core sample. Subsequently, over a two-week period, the pressure was gradually increased to the experimental conditions of 80 bar using low nutrient gas supply rates. Fig. 8 presents the chemical analysis of the gas phase at the core outlet as well as pressure, flow rate, and pH measurements recorded during the inoculation phase prior to the first dispersion test with microbial culture.

Over time, decreasing concentrations of H_2 and CO_2 were observed at the outlet, accompanied by an increasing fraction of biogenic CH_4, indicating a progressive increase in the metabolic activity of the in-situ microbial community. Throughout the inoculation period, pH measurements remained stable and showed no indication of acidification, suggesting that no metabolic shift toward acetogenesis occurred.

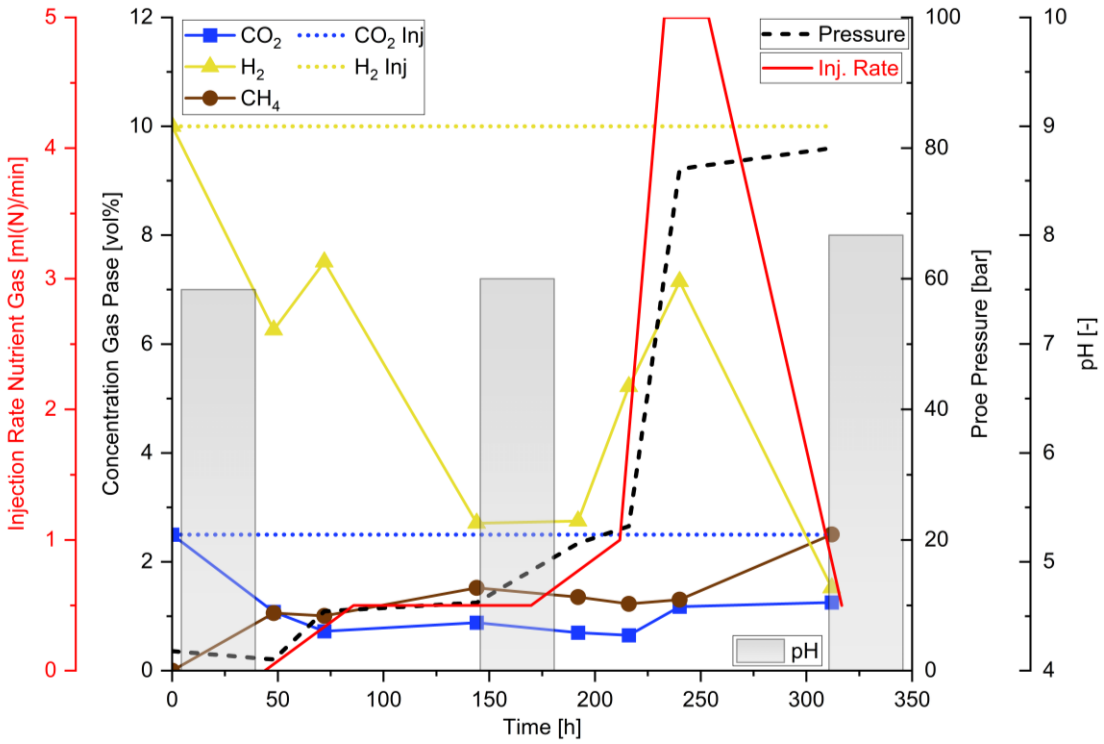

Fig. 8: Inoculation of the core sample with a methanogenic consortium. Volume concentrations of H_2, CO_2, and CH_4 were measured at the outlet via gas chromatography (GC). The horizontal dotted lines represent the concentrations of the injected gas mixture. Additionally, the injection rate (solid red line), the pressure buildup (dashed black line), and the pH monitoring (gray bars) are displayed over a period of 2 weeks.

A clear upward trend in methane concentration is evident, which is only interrupted between 200 and 250 hours. This transient decrease is attributed to an increased injection rate, which reduced the residence time available for the conversion of the fresh nutrient gas.

Following the inoculation phase, the brine saturation was reduced to a quasi-immobile level as described above, and the core was purged with nitrogen gas. This state served as the initial condition for the dispersion experiments, with a CT scan performed prior to test period, to define the saturation state.

In Fig. 6, alongside the effects of CO_2 solubility in the aqueous phase, the microbial consumption of this gas component can be clearly observed. In the experiment utilizing the dry core sample, a relatively rapid equilibration to the initially injected CO_2 concentration of 2.5% is detected at the outlet via GC analysis after the breakthrough (orange curve). In the brine-saturated experiment (blue curve), a temporal shift is discernible due to the dissolution reaction; however, a delayed equilibration to the injected CO_2 concentration is subsequently observed. A contrasting scenario is presented by the green curve, which represents the experiment with the biologically active substrate: here, the CO_2 concentration at the outlet stabilizes after breakthrough at approximately 1.5% CO_2, which is roughly 1% lower compared to the injected gas mixture. Consequently, this deficit is attributable to the consumption and metabolism by the methanogenic microorganisms.

Fig. 7 illustrates also the reduction of Hydrogen at the outlet in addition to the microbial utilization of CO_2. Furthermore, the biochemically converted methane concentration (brown line) is plotted. Across all experiments featuring active microorganisms within the core sample under the given conditions and a constant injection rate of 2.99 mL(n)/min, the following alterations in gas composition were observed at the outlet after breakthrough of the injected gas mixture:

- A reduction in CO_2 concentration from 2.49% to 1.5 - 1.7%
- A reduction in H_2 concentration from 9.97% to 8.7 - 9.2%
- A conversion to methane resulting in concentrations of 0.15 - 0.25%

These changes in concentration indicate an active methanogenic metabolism of the inoculated consortium. The deviation from the exact stoichiometric ratio of the reaction (4 mole H_2 and 1 mole CO_2 to 1 mole CH_4, see Eq. 1) can be attributed to the synthesis of new biomass and cellular growth. The highly complex processes within a microbial consortium encompass not only the pure metabolic reaction for energy generation

(methanogenesis) but also the production and transformation of new organic structures, as well as the degradation and utilization of deceased cellular material.

A measurable indicator of excessive biomass proliferation is the alteration of hydraulic parameters. By measuring the differential pressure, the reduction in permeability can be determined. The values presented in Fig. 9 represent the single-phase permeability of a fully brine-saturated core sample. A comparison between the initial brine saturated state and the state following the inoculation of the methanogenic consortium, including a 3-week growth phase and the execution of dispersion experiments, demonstrates a 50% reduction of the permeability.

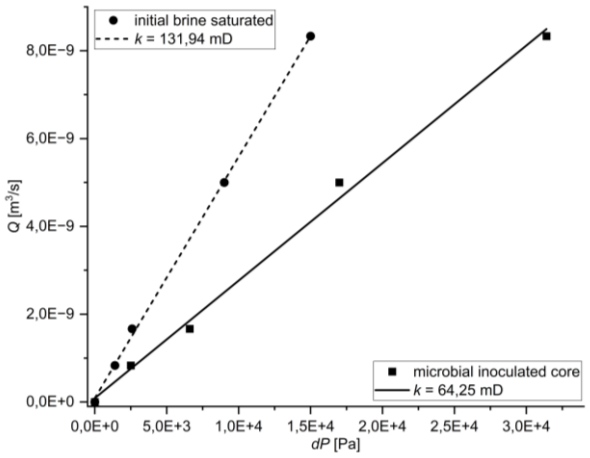

Fig. 9: Comparison of permeability for the core under initial brine-saturated and microbially inoculated conditions. The data illustrates a permeability reduction of 50%. Permeability values were determined via Darcy's law for single-phase flow based on differential pressure measurements at alternating flow rates

The permeability reduction observed in the core-flooding experiments using the same microbial consortium is consistent with the pore-scale observations reported by [25], in which microbial growth induced significant porosity and permeability alterations through biomass accumulation and partial pore-throat clogging. Compared to quasi-2D microfluidic systems, natural rocks exhibit higher tortuosity, more confined pore throats, dead-end pores, and limited bypass pathways, increasing the susceptibility to bio-clogging and flow redistribution. Consequently, microbial growth in reservoir rocks may lead to greater reductions in effective permeability and injectivity, even when only moderate porosity losses occur.

However, the quantity of converted methane depends not only on the precise experimental conditions but also on the injection rate; or rather, the residence time of the gas within the pore space of the core serving as the reactor space. To establish a degree of comparability with other studies, a reactor efficiency (r_V) was determined from the generated methane concentrations. For this purpose, the methane concentration after breakthrough was integrated over the remaining duration of the experiment and normalized to the available pore volume within the core sample. This yields the quantity of methane generated per unit volume and unit time, referred to as the pore volume-normalized rate:

$$r_V = \frac{n_{CH_4}}{V_{Pore} t} \quad [mmol L^{-1} h^{-1}] \qquad (5)$$

This normalization eliminates geometric scale effects and enables benchmarking against alternative experimental approaches. The resulting formation rates of the experiments described herein are in the range of $r_V = (0.178 - 0.284)$ mmol L^{-1} h^{-1}. To establish a cross-scale evaluation of the in-situ methanation potential, this reactor efficiency at the meso-scale was compared with pore-scale experiments and numerical field-scale simulations [2], [31], [32].

The resulting rates agree within ~23%, which is within expected experimental and biological variability and indicates that apparent methane production might be not vastly scale-dependent when expressed per pore volume and time. Differences in injected gas composition and operating pressure were further examined by considering reactant partial pressures [32].

4 Conclusion and Outlook

This study investigated dispersive transport processes and microbial conversion mechanisms relevant to underground hydrogen storage (UHS) and subsurface geo-methanation under representative reservoir conditions. Through a systematic experimental approach with increasing complexity, ranging from dry gas-gas displacement to partially brine-saturated systems and finally biologically active porous media, the coupled influence of hydrodynamic dispersion, gas solubility, and microbial activity on gas transport and conversion behavior was quantified.

The experiments demonstrated that the presence of an immobile aqueous phase significantly alters dispersion characteristics compared to dry porous media. At low flow velocities, reduced effective diffusion dominated the transport behavior, whereas at higher velocities increased dispersivity due to reduced gas-filled pore space and enhanced tortuosity became the controlling mechanism. These findings highlight the strong dependency of effective transport coefficients on fluid saturation conditions and emphasize the necessity of considering multiphase effects when evaluating UHS performance.

A pronounced retardation of CO_2 breakthrough relative to H_2 was observed in all experiments involving a stationary brine phase. The measured temporal shift corresponded closely to the theoretically expected dissolution capacity of CO_2 in the brine, indicating that gas solubility exerts a first-order control on reactive transport processes in partially saturated reservoirs. In contrast, hydrogen solubility remained negligible under the investigated conditions and showed no measurable influence on the overall gas composition.

In the presence of active methanogenic cultures, additional deviations in gas composition confirmed ongoing biological conversion processes. The reduction of H_2 and CO_2 concentrations together with the simultaneous formation of CH_4 demonstrated active hydrogenotrophic methanogenesis within the porous medium. The observed methane formation rates were consistent with previously reported laboratory- and field-scale studies, suggesting that pore-volume-normalized conversion rates may provide a scalable parameter for evaluating in-situ methanation performance across different experimental scales.

Beyond the biochemical conversion itself, the experiments revealed substantial changes in hydraulic properties caused by microbial growth. The measured permeability reduction of approximately 50% indicates significant biomass accumulation and bio-clogging effects within the pore structure. This demonstrates that microbial activity not only alters gas composition but may also progressively modify reservoir injectivity and flow behavior over time. Consequently, microbial growth must be considered as both a potential opportunity for renewable methane generation and a possible operational challenge for long-term hydrogen storage.

Future work should focus on extending these investigations toward a more detailed characterization of the influence of rock heterogeneity and spatial water phase distribution on dispersive transport and microbial conversion processes. In particular, variations in porosity, permeability, and local saturation conditions are expected to significantly affect gas mixing behavior, substrate accessibility, and biomass development within the porous medium. Furthermore, numerical reservoir simulations will be employed to history-match the experimental data obtained in this study. The integration of experimentally derived transport coefficients and reaction parameters into reactive transport models will enable improved prediction of coupled hydrodynamic and biogeochemical processes and support the upscaling of laboratory observations to field-scale underground hydrogen storage and geo-methanation applications.

Abbreviations

ADE = advection–dispersion equation
ADR = advection-dispersion-reaction equation
CCU = carbon capture and utilization
CT = computed tomography
GC = gas chromatography
PV = pore volume
PV_{Gas} = free gas pore volume
RSD = relative standard deviation
UHS = underground hydrogen storage

Symbols

α = longitudinal dispersivity, m
CT_{Core}^{i} = CT number at timestep i, Houndsfield units
C = molar concentration, mol/mol
D = dispersion coefficient, m²/s
D_{bulk}^{AB} = binary gas-gas diffusion coefficient, m²/s
D_{eff}^{AB} = effective gas-gas diffusion coefficient, m²/s
D_{eff} = effective dispersion coefficient, m²/s
μ = dynamic viscosity, Pa.s
Pe = Peclet number
ϕ = porosity
r_V = methane formation rate, mmol L^{-1} h^{-1}
S_{brine} = brine saturation
S_g = gas saturation
t = time, s
t_D = dimensionless time
u = average fluid velocity, m/s
u_{int} = interstitial velocity, m/s

References

[1] M. Pichler, H. Konegger, A. Loibner, S. Bauer, *Final Report: Underground Sun Conversion* (2021)
[2] M. Abdellatif, S. Azizmohammadi, G. Stiedl, M. Pichler, H. Ott, Int. J. Hydrogen Energy, **105**, 1164–1177 (2025)
[3] R. Tarkowski, B. Uliasz-Misiak, Renew. Sustain. Energy Rev., **162**, 112451 (2022)
[4] P. Šmigáň, M. Greksák, J. Kozánková, F. Buzek, V. Onderka, I. Wolf, FEMS Microbiol. Lett., **73**, 221–224 (1990)
[5] K. Coyte, H. Tabuteau, E. Gaffney, K. Foster, W. Durham, Proc. Natl. Acad. Sci. U.S.A., **114** (2016)
[6] N. Hassannayebi, S. Azizmohammadi, M. De Lucia, H. Ott, Environ. Earth Sci., **78** (2019)
[7] E.M. Thaysen et al., Renew. Sustain. Energy Rev., **151**, 111481 (2021)
[8] H.Y. Jeong, S.-C. Jun, J.-Y. Cheon, M. Park, Geosci. J., **22**, 667–679 (2018)
[9] J. Delgado, Heat Mass Transfer, **42**, 279–310 (2006)
[10] A. Kumar, D.K. Jaiswal, N. Kumar, J. Hydrol., **380**, 330–337 (2010)
[11] J. Bear, A. Cheng, *Modeling Groundwater Flow and Contaminant Transport* (Springer, 2010)
[12] P. Atkins, J. de Paula, *Physical Chemistry*, 10th ed. (Oxford University Press, Oxford, 2014)
[13] R. Sander, Atmos. Chem. Phys., **15**, 4399–4981 (2015)
[14] P. Jasek, G. Stiedl, H. Ott, Int. J. Hydrogen Energy, **250**, 155834 (2026)
[15] *Equilibar Research Series Back Pressure Regulators* (Equilibar LLC, Fletcher, 2025)
[16] G. Stiedl, H. Ott, B. Jammernegg, in *38th International Symposium of the Society of Core Analysts* (Hannover, 2025), SCA2025-1055
[17] X. Miao, Y. Wang, L. Zhang, N. Wei, X. Li, Micron, **124**, 102703 (2019)
[18] H. Ott, S. Oedai, Geophys. Res. Lett., **42**, 2270–2276 (2015)

[19] J. Zhang, *Application Note: Analysis of Fischer-Tropsch Syngas and Tail Gas with the Agilent 990 Micro GC* (Agilent Technologies, 2023)
[20] *Datasheet M12 Coriolis Mass Flow Meter for Liquids and Gases* (Bronkhorst High-Tech B.V., Ruurlo, 2025)
[21] H.J. Vinegar, S.L. Wellington, Rev. Sci. Instrum., **58**, 96–107 (1987)
[22] *SOMATOM Definition AS: Technical Data* (Siemens Healthineers, Erlangen, 2012)
[23] S. Berg, S. Oedai, and H. Ott, Int J. of Greenhouse Gas Control, **12**, 478–492, (2013)
[24] S. Berg et al., Petrophysics - SPWLA J. **55**, 304–312 (2014)
[25] P. Jasek, H. Konegger, A.P. Loibner, H. Ott, Int. J. Hydrogen Energy **157**, 150191 (2025)
[26] N.H. Chen, D.F. Othmer, J. Chem. Eng. Data **7**, 37–41 (1962)
[27] M.S. Costanza-Robinson, M.L. Brusseau, in *Gas Transport in Porous Media*, ed. by C.K. Ho, S.W. Webb (Springer Netherlands, Dordrecht, 2006), pp. 121–132
[28] J. Michelsen, N. Langanke, B. Hagemann, S. Hogeweg, L. Ganzer, in *Advanced SCAL for Carbon Storage & CO_2 Utilization* (2023)
[29] J.B. Burkholder et al., in *AGU Fall Meeting Abstracts* **2015**, A21B-0130 (2015)
[30] R. Sander, Atmos. Chem. Phys. **23**, 10901–12440 (2023)
[31] P. Jasek, G. Stiedl, S. Hochmeister, J. Kulich, H. Ott, Eur. Phys. J. Appl. Phys. (to be published)